

## Article

# Electrophysiological Activity of Primary Cortical Neuron-Glia Mixed Cultures

Noah Goshi <sup>1</sup> , Hye Hyun Kim <sup>1</sup>, Gregory Girardi <sup>1</sup>, Alexander Gardner <sup>2</sup> and Erkin Seker <sup>2,\*</sup> 

<sup>1</sup> Department of Biomedical Engineering, University of California—Davis, Davis, CA 95616, USA

<sup>2</sup> Department of Electrical and Computer Engineering, University of California—Davis, Davis, CA 95616, USA

\* Correspondence: eseker@ucdavis.edu

**Abstract:** Neuroinflammation plays a central role in many neurological disorders, ranging from traumatic brain injuries to neurodegeneration. Electrophysiological activity is an essential measure of neuronal function, which is influenced by neuroinflammation. In order to study neuroinflammation and its electrophysiological fingerprints, there is a need for in vitro models that accurately capture the in vivo phenomena. In this study, we employed a new tri-culture of primary rat neurons, astrocytes, and microglia in combination with extracellular electrophysiological recording techniques using multiple electrode arrays (MEAs) to determine the effect of microglia on neural function and the response to neuroinflammatory stimuli. Specifically, we established the tri-culture and its corresponding neuron-astrocyte co-culture (lacking microglia) counterpart on custom MEAs and monitored their electrophysiological activity for 21 days to assess culture maturation and network formation. As a complementary assessment, we quantified synaptic puncta and averaged spike waveforms to determine the difference in excitatory to inhibitory neuron ratio (E/I ratio) of the neurons. The results demonstrate that the microglia in the tri-culture do not disrupt neural network formation and stability and may be a better representation of the in vivo rat cortex due to its more similar E/I ratio as compared to more traditional isolated neuron and neuron-astrocyte co-cultures. In addition, only the tri-culture displayed a significant decrease in both the number of active channels and spike frequency following pro-inflammatory lipopolysaccharide exposure, highlighting the critical role of microglia in capturing electrophysiological manifestations of a representative neuroinflammatory insult. We expect the demonstrated technology to assist in studying various brain disease mechanisms.

**Keywords:** neuron; astrocyte; microglia; primary cell culture; in vitro model; neuroinflammation; microelectrode array; extracellular recordings; neural network; electrophysiology



**Citation:** Goshi, N.; Kim, H.; Girardi, G.; Gardner, A.; Seker, E. Electrophysiological Activity of Primary Cortical Neuron-Glia Mixed Cultures. *Cells* **2023**, *12*, 821. <https://doi.org/10.3390/cells12050821>

Academic Editors: Andrew Chih Wei Huang, Seong Soo A. An, Bai Chuang Shyu, Muh-Shi Lin and Anna Kozłowska

Received: 23 January 2023

Revised: 17 February 2023

Accepted: 28 February 2023

Published: 6 March 2023



**Copyright:** © 2023 by the authors. Licensee MDPI, Basel, Switzerland. This article is an open access article distributed under the terms and conditions of the Creative Commons Attribution (CC BY) license (<https://creativecommons.org/licenses/by/4.0/>).

## 1. Introduction

In vitro models of the central nervous system (CNS) are powerful tools that allow researchers to conduct highly directed cellular-level experiments to study the cellular and molecular pathways underlying many neurological disorders. However, there are inherent limitations within these models that limit their physiological relevance. Most notably, researchers must ensure that the appropriate cell types are included within their culture model to effectively recapitulate the in vivo disease state. This is especially true for CNS models as crosstalk between neurons and glia play significant roles in both pathological conditions [1–5] and maintaining homeostasis [6,7]. The microelectrode array (MEA) technology is a popular method to study in vitro neural networks, as it provides a non-invasive method to simultaneously record electrophysiological activity from multiple sites [8,9]. This allows researchers to conduct longitudinal studies to study neural network formation [10,11] and disruption caused by neurotoxic compounds [12–14] and proteins associated with neurodegeneration [15–17]. Nevertheless, the physiological relevance of these studies is still largely dependent on the cell types present within the culture and may not

fully recapitulate the *in vivo* response [18]. Therefore, there have been significant efforts in developing new CNS culture models and characterizing the spatial and temporal aspects of electrophysiological recordings both during spontaneous activity and in response to stimuli. This includes studying the neural activity from cultures of neurons from different regions of the brain (cortex [8,19,20] vs. hippocampus [21,22]), neurons cultured with supporting glial cells such as astrocytes [23] and oligodendrocytes [24], and human primary [25] or stem cell-derived [26,27] neurons. Additionally, electrophysiological recording from complex *in vitro* models such as 3D [28,29] and organ-on-a-chip [30,31] models have been studied to further improve the physiological relevance of *in vitro* neural models.

We have previously developed a neuron, astrocyte, and microglia tri-culture to study neuroinflammation *in vitro* [32]. This tri-culture is maintained by culturing primary cortical neurons from neonatal rats in a serum-free culture medium specifically designed to support all three cell types. We have demonstrated that the tri-culture model better mimics the neuroinflammatory response to a number of stimuli, including lipopolysaccharide (LPS) exposure, mechanical trauma, glutamate-induced excitotoxicity, and toll-like receptor (TLR) activation [32,33] as compared to neuron-astrocyte co-cultures, which is a common method to study neuroinflammation *in vitro* [34]. In this paper, we further explore the capabilities of the tri-culture by characterizing the neural functionality of the system. We compared the extracellular recordings taken over 21 days *in vitro* (DIV) between the tri- and co-cultures to determine the effect of microglia on network formation and neuron function. We demonstrate that many features of neural activity remain similar between the tri- and co-cultures (% active channels, spike frequency, and burst characteristics), suggesting that the presence of microglia does not adversely affect neuronal function. Additionally, an analysis of the action potential waveform characteristics reveals that the tri-cultures contain an increased excitatory/inhibitory (E/I) neuron ratio that more closely resembles the ratio found *in vivo*; this observation is supported by synaptic staining. We also incorporated the tri-culture into compartmentalized organ-on-a-chip devices that separate the neural axons and somas using microchannels [31,35] and recorded robust neural activity from these platforms. Finally, we demonstrate the ability to observe changes in neural activity in response to known inflammatory stimuli (LPS exposure).

## 2. Materials and Methods

### 2.1. MEA Design and Fabrication

Custom MEAs and microfluidic platforms were fabricated using previously described methods [31]. Briefly, standard (well) MEAs were designed with a  $4 \times 8$  array of electrodes (32 total) each with a diameter ( $\varnothing$ ) of 20  $\mu\text{m}$  and an interelectrode pitch of 130  $\mu\text{m}$ . The electrodes and traces (250 nm-thick Au over a 160 nm-thick Cr adhesion layer) were sputter-deposited on borosilicate glass wafers (500  $\mu\text{m}$  thick, University Wafers) and patterned using standard lift-off techniques.  $\text{SiO}_2$  was deposited via PECVD to serve as the insulation layer. Finally, the electrode sites were lithographically patterned and opened via a brief immersion in buffered oxide etch. Glass cloning cylinders (8 mm  $\times$  6 mm inner  $\varnothing$ , Sigma, MI, USA) were then attached over the MEA using sterile vacuum grease (Dow Corning, Midland, MI, USA).

Microfluidic platforms were designed following recommendations from our previous study [31]. Polydimethylsiloxane (PDMS; Sylgard 184, Dow Corning, Midland, MI, USA) microfluidic devices were fabricated using standard soft-lithography techniques. These devices contained two large cell culture chambers connected by 101 microchannels with dimensions of 1000  $\mu\text{m} \times 10 \mu\text{m} \times 1.5 \mu\text{m}$  (length  $\times$  width  $\times$  height). These microchannels allowed axons, but not somas of neurons, to enter the microchannels and, thereby, synaptically connect the two separate neural populations. Corresponding MEAs with an array of eight microchannels in each cell culture chamber and an array of 16 electrodes placed under the microchannels were fabricated using the same methods as above. To form the final device, both the MEA and PDMS platforms were sterilized with 70% EtOH, and the surfaces were activated with air plasma at 10 W for 2 min. The MEA was then covered

with 70% EtOH, and the PDMS platform was placed over the MEA and aligned under a microscope. The aligned device was placed in a vacuum chamber for 1 h to remove the EtOH solution and permanently bond the MEA and PDMS platform. The bonded devices were then treated with air plasma at 30 W for 10 min to make the surfaces hydrophilic, and glass cloning cylinders were mounted over the fluidic ports.

## 2.2. Primary Cortical Culture

All media were prepared as previously described [19,32]. Briefly, plating medium consisted of Neurobasal A culture medium supplemented with 2% B27 supplement, 1x GlutaMAX, 10% heat-inactivated horse serum, and 20 mM HEPES at pH 7.5, while the co-culture medium consisted of Neurobasal A culture medium supplemented with 2% B27 supplement and 1x GlutaMAX (all from ThermoFisher, Waltham, MA, USA). The tri-culture medium consisted of supplementing the co-culture medium with 100 ng/mL mouse IL-34 (R&D Systems, Minneapolis, MN, USA), 2 ng/mL TGF- $\beta$  (Peprotech, Cranbury, NJ, USA), and 1.5  $\mu$ g/mL ovine wool cholesterol (Avanti Polar Lipids, Alabaster, AL, USA), which were identified as factors that support isolated microglia survival in culture [36]. Due to the limited shelf life of IL-34 and TGF- $\beta$ , the tri-culture medium was made fresh each week.

All procedures involving animals were conducted in accordance with the National Institutes of Health Guide for the Care and Use of Laboratory Animals following protocols approved by the University of California, Davis Institutional Animal Care and Use Committee. Timed-pregnant Sprague–Dawley rats were purchased from Charles River Laboratory (Hollister, CA, USA). All animals were housed in clear plastic shoebox cages containing corn cob bedding under constant temperature ( $22 \pm 2$  °C) and a 12 h light–dark cycle. Food and water were provided ad libitum. Primary cortical cultures were prepared from postnatal Day 0 rat pups as previously described [37]. Neocortices from all pups in the litter were pooled, dissociated, and resuspended in plating medium. Prior to plating, all substrates were coated with 0.5 mg/mL poly-L-lysine (Sigma-Aldrich, St. Louis, MO, USA) in B-buffer (3.1 mg/mL boric acid and 4.75 mg/mL borax, Sigma-Aldrich, St. Louis, MO, USA) for 4 h at 37 °C and 5% CO<sub>2</sub>, and then washed with sterile deionized water and covered with plating medium. Cultures were plated at a density of 550 cells/mm<sup>2</sup> on well MEAs (Figure 1), while for the microfluidic devices, 20  $\mu$ L of cell suspension at a concentration of  $3 \times 10^6$  cells/mL were seeded in each chamber (Figure 2). The cells were allowed to adhere for 4 h, after which the plating medium was changed to tri- or co-culture medium. Half-media changes were performed every 3–4 days with the respective media types.

## 2.3. Immunocytochemistry

At the conclusion of the experiment, the cell cultures were washed three times with 37 °C DPBS+ and fixed using 4% *w/v* paraformaldehyde (PFA; Affymetrix, Santa Clara, CA, USA) in PBS for 2.5 h. Fixed cells were washed twice with 0.05% *v/v* Tween20 (Sigma) solution in DPBS+, followed by a 3 min permeabilization with 0.1% *v/v* Triton X-100 (ThermoFisher, Waltham, MA, USA) solution in DPBS+ and two additional washes with Tween20 solution. Samples were blocked with a solution of 0.5% *v/v* heat-inactivated goat serum (ThermoFisher, Waltham, MA, USA) and 0.3 M glycine (Sigma-Aldrich, St. Louis, MO, USA) in DPBS+ (blocking buffer) for 1 h. Following the blocking step, samples were incubated for 1 h in primary antibody solution containing mouse anti-PSD-95 (ThermoFisher, Waltham, MA, USA), rabbit anti-VGlut1 (ThermoFisher, Waltham, MA, USA), and chicken anti-MAP2 (Abcam, Waltham, MA, USA) in blocking buffer. Alternatively, some samples were incubated with mouse anti- $\beta$ III tubulin (ThermoFisher, Waltham, MA, USA), rabbit anti-GFAP (ThermoFisher, Waltham, MA, USA), and chicken anti-Iba1 (Abcam, Waltham, MA, USA) to ensure the cellular compositions of the culture. Samples were then washed three times with Tween20 solution before a 1 h incubation with secondary antibody solution containing goat anti-mouse antibodies conjugated to AlexaFluor 647 (ThermoFisher, Waltham, MA, USA), goat anti-rabbit antibodies conjugated to AlexaFluor 488 (ThermoFisher, Waltham, MA, USA), and goat anti-chicken antibodies conjugated to AlexaFluor 555 (ThermoFisher,

Waltham, MA, USA). Following incubation with secondary antibody solution, the samples were washed three times with DPBS+. Lastly, samples were incubated for 5 min with a 4',6-diamidino-2-phenylindole (DAPI) solution (Sigma-Aldrich, St. Louis, MO, USA) to stain cell nuclei, followed by an additional Tween20 solution wash before mounting them onto glass slides using ProLong Gold Antifade Mountant (ThermoFisher, Waltham, MA, USA).

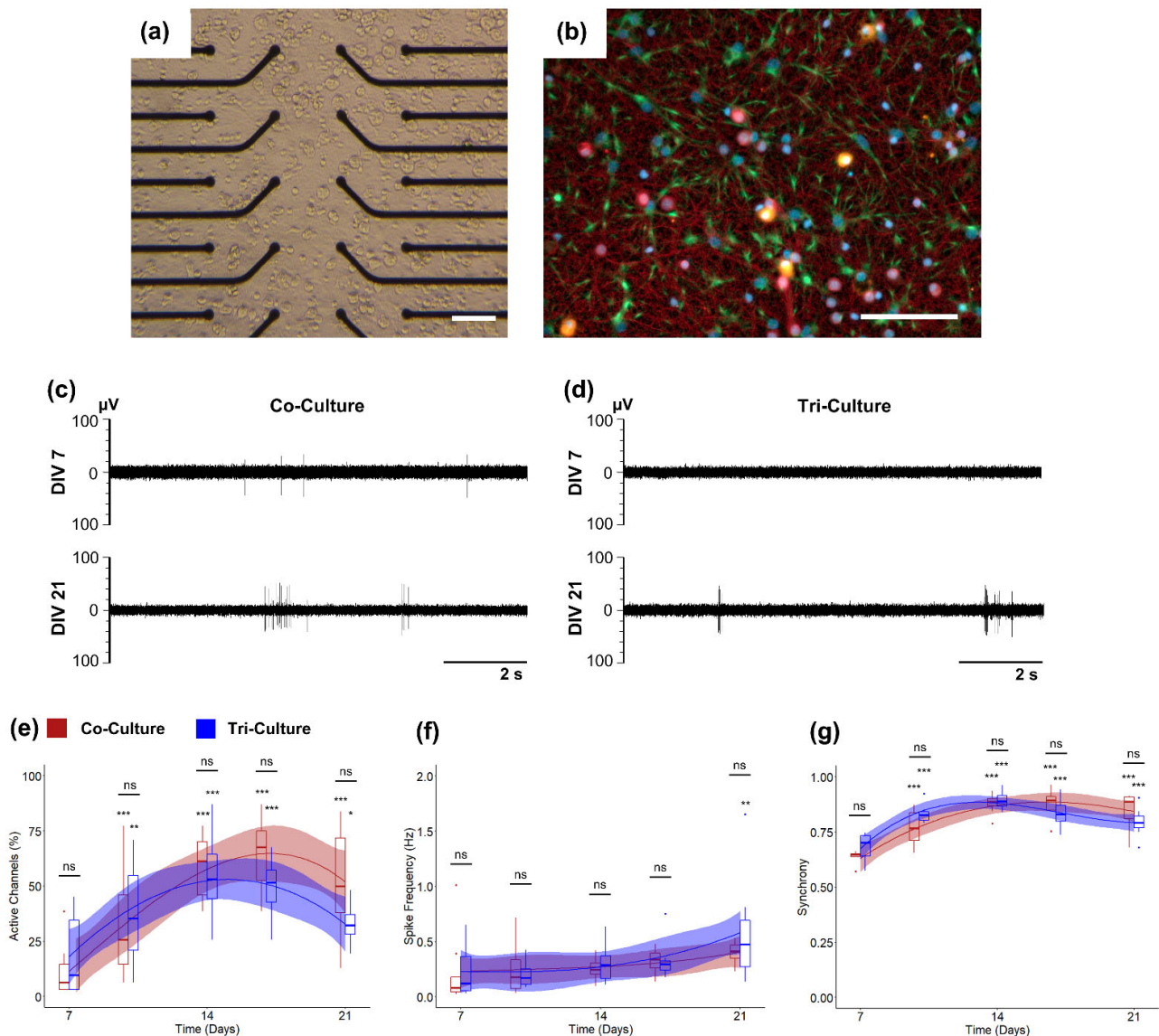


**Figure 1.** (a) Bright-field and (b) epifluorescence images of the tri-culture at DIV 21 on the well MEA. The cultures were immunostained for the three cell types of interest: neurons—anti- $\beta$ III-tubulin (red), astrocytes—anti-GFAP (green), microglia—anti-Iba1 (orange), and the general nuclear stain DAPI (blue). (Scale bar = 100  $\mu$ m). Representative extracellular recordings taken at DIV 7 and DIV 21 from (c) co-cultures and (d) tri-cultures. Comparisons of the (e) percentage of active channels, (f) spike frequency, and (g) synchrony between co-cultures (red) and tri-cultures (blue). The solid lines show the fitted linear mixed effects model (treating individual cultures as a random effect) with a b-spline basis. The shaded regions are the 95% confidence interval. An asterisk above an individual box indicates a significant difference of the estimated marginal means of the fitted curves between that timepoint and DIV 7 of the same culture type, while the bars indicate the significance between the co- and tri-culture at that timepoint ( $n = 8$ , from three independent dissections). \*  $p < 0.05$ , \*\*  $p < 0.01$ , \*\*\*  $p < 0.001$ , ns indicates no significant difference. Scale bar = 100  $\mu$ m.



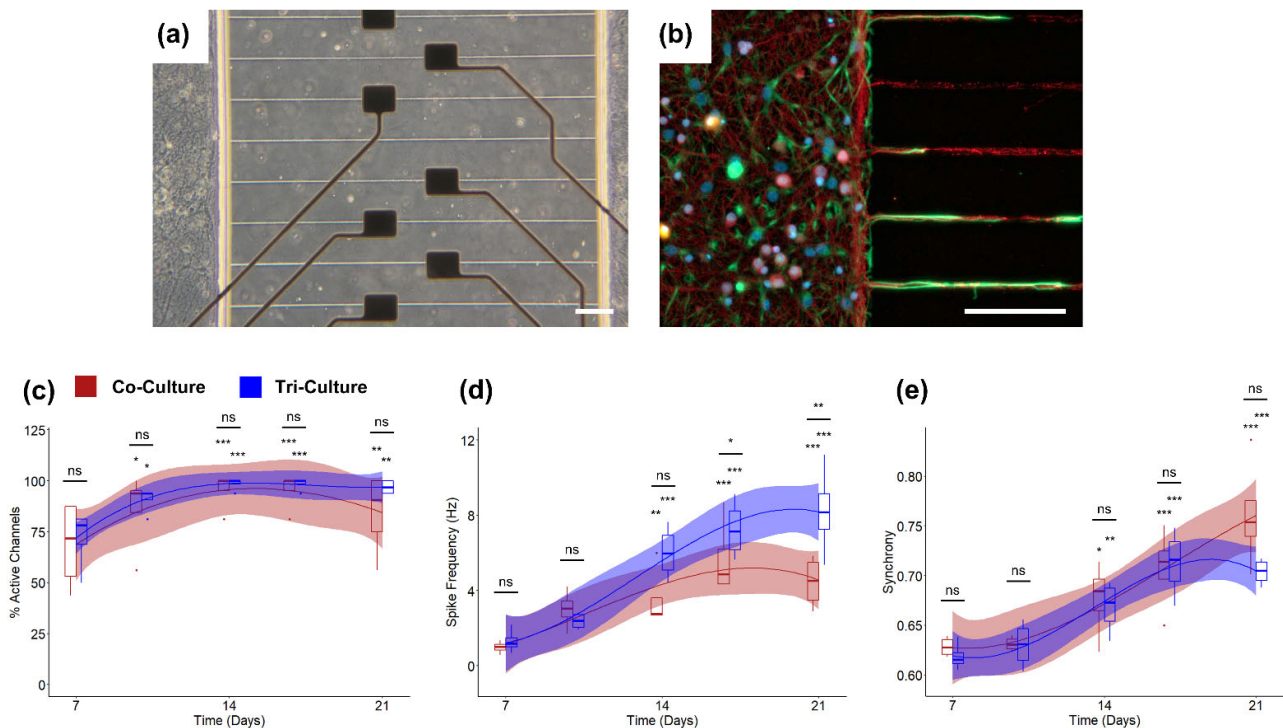


**Figure 2.** (a) Bright-field and (b) epifluorescence images of the tri-culture at DIV 21 in the platform MEA with microfluidic encapsulation. The cultures were immunostained for the three cell types of interest: neurons—anti- $\beta$ III-tubulin (red), astrocytes—anti-GFAP (green), microglia—anti-Iba1 (orange), and the general nuclear stain DAPI (blue). (Scale bar = 100  $\mu$ m). Comparisons of the (c) percent active channels, (d) spike frequency, and (e) synchrony between co-cultures (red) and tri-cultures (blue) cultured in a two-chambered microfluidic device. The solid lines show the fitted linear mixed effects model (treating individual cultures as a random effect) with a b-spline basis. The shaded regions are the 95% confidence interval. An asterisk above an individual box indicates a significant difference of the estimated marginal means of the fitted curves between that timepoint and DIV 7 of the same culture type, while the bars indicate the significance between the co- and tri-culture at that timepoint ( $n = 5$ , from two independent dissections). \*  $p < 0.05$ , \*\*  $p < 0.01$ , \*\*\*  $p < 0.001$ , ns indicates no significant difference.

#### 2.4. Image Analysis

All sample images were acquired using a Leica TCS SP8 STED 3X microscope (Leica Microsystems, Deerfield, IL, USA) with a 63x/1.4 oil immersion objective and analyzed using a custom ImageJ macro [32]. Briefly, the images were thresholded to determine the number of pre- and post-synaptic puncta, and the number of mature synapses were quantified by determining the number of co-localized puncta. These values were then correlated with dendrite length to determine the number of puncta or mature synapses per 100  $\mu$ m of dendrite length. For all analysis, five predetermined fields were analyzed per well to account for variability within the individual cultures.

#### 2.5. Electrophysiological Recording and Analysis

For extracellular electrophysiological recordings, the devices were placed on a custom-built rig and maintained at 37  $^{\circ}$ C and 5% CO<sub>2</sub> during the recordings. Recordings were performed at a sampling frequency of 30 kHz using an RHD2132 Intan amplifier (Intan Technologies, Los Angeles, CA, USA). Half-media changes were performed 24 h prior to each recording except for LPS-treated conditions (LPS from *E. coli* O111:B4; Invivogen, tlr1-eb1ps, San Diego, CA, USA), in which the half-media change was performed 24 h prior to the baseline measurement. Feature extraction from the recordings was done using Offline Sorter and NeuroExplorer Version 5.310 (Plexon, Dallas, TX, USA). Spikes

were detected following high-pass filtering (300 Hz cut-off) using a threshold of  $\pm 8 \times$  standard deviation of the noise. Channels that showed less than 10 spikes per 10 min of recording were discarded from the analysis. The number of active electrodes for each array was determined as the number of electrodes that registered at least 10 spikes during the 10-min recording. Overall synchrony of the active electrodes within each device was determined using the SPIKE-distance methodology [38] in the PySpike Python package [39]. Bursts were classified using the max interval method in NeuroExplorer using previously defined parameters [24,40]. Briefly, these parameters were: (i) Maximum initial inter-spike interval (ISI) of 0.1 s; (ii) Maximum end ISI of 0.25 s; (iii) Minimum inter-burst interval of 0.5 s; (iv) Minimum burst duration of 0.05 s; and (v) Minimum number of spikes in bursts of six spikes. They were used to determine the percentage of spikes in bursts, average burst duration, and average interspike interval (ISI) within bursts at a per-electrode basis. Spike frequency and burst features were determined on a per-electrode basis, but statistical analysis was performed on a per-device basis by taking the overall mean from the active electrodes.

To determine the average peak-trough duration, we first sorted the extracted spikes using the valley-seeking algorithm in OfflineSorter Version 4.6.2 (Plexon, Dallas, TX, USA) with a Parzen multiplier of 2.0. Due to the relatively large distance between the electrodes and low seeding density, nearly every electrode only displayed one cluster. However, on occasion, two duplicate clusters were found due to the use of dual thresholds during spike detection ( $\pm 8\sigma$ ). As these two clusters clearly belonged to the same group, one cluster was disregarded from the analysis. The average peak-trough duration of each cluster was then calculated via OfflineSorter.

## 2.6. Statistical Analysis

To compare change in the different spike features based on culture type or condition, each dataset was fitted using a linear mixed effects model (treating the individual devices as a random effect) with a b-spline basis to account for the overall shape of the plots [31]. We then compared the estimated marginal means from the fitted curves at each timepoint and adjusted for multiple comparisons using the Holm–Bonferroni method. A two-way ANOVA was used to compare the differences in synaptic staining over time, while a Student's *t*-test was used to compare the differences in peak-trough duration between the tri- and co-culture at DIV 21. For all experiments, statistical significance was determined by *p*-values  $< 0.05$ . Furthermore, unless otherwise noted, for experiments requiring image analysis, at least five predetermined fields were analyzed per replicate to account for variability within the culture itself. As the cortices from each litter was pooled prior to dissociation and plating, and each well or MEA was treated individually, all experiments were performed with a minimum  $n = 4$  from at least two independent dissections [41].

## 3. Results

### 3.1. Electrophysiology

We recorded spontaneous neural activity from DIV 7 to DIV 21 from both tri- and co-cultures to determine if there was any discernible difference in culture maturation or network formation (Figure 1c,d). As expected, we observed a significant increase in the percentage of active channels in both the tri- and co-culture from DIV 7 to DIV 21 (Figure 1e). However, we did not find a significant difference in the percentage of active channels between the tri- and co-cultures at any timepoint. We saw a similar trend in spike frequency for both the tri- and co-cultures (Figure 1f), with no differences between the tri- and co-cultures. However, in this case, the increase in spike frequency is less pronounced. Therefore, we did not observe a significant increase between DIV 7 and later timepoints, with the exception of the tri-culture at DIV 21 ( $p = 0.0076$ ). We also compared other electrophysiological features used to determine culture maturation and stability over time (Figure S1), such as the percentage of spikes in bursts, burst duration, and ISI within bursts. Both the tri- and co-cultures showed a significant increase in the percentage of

spikes in bursts, indicating that the cultures were maturing as expected; however, there was no difference between the two cultures (Figure S1a). Similarly, we saw no difference between the average burst duration and within burst ISI between the two culture types (Figure S1b,c). For both the co- and tri-culture, these values remained stable over time, suggesting no degradation in neural health over the 21 DIV window. Finally, we compared network formation in the tri- and co-cultures by assessing the synchrony of the spike trains from the active electrodes in each culture using the SPIKE-distance method [38,39]. It is important to note that the SPIKE-distance method is a measurement of spike-train dissimilarity given on a scale of 0–1. Therefore, in order to measure the synchrony of the culture, we subtracted the SPIKE distance value from 1, with values closer to 1 indicating increased synchrony in the culture. We observed a significant increase in synchrony over time in both the co- and tri-cultures, indicating robust network formation (Figure 1g). While there was no significant difference in the synchrony between the tri- and co-culture, there was a trend towards increased synchrony in the tri-culture at DIV 10 ( $p = 0.11$ ).

### 3.2. Incorporation into Microfluidic Platforms

In order to further investigate some of the non-statistically significant but important trends we previously observed, we compared the spontaneous neural activity from tri- and co-cultures maintained in microfluidic devices (Figure 2a,b), which were previously shown to improve electrophysiological recording fidelity [31,42,43]. We once again demonstrated that both the tri- and co-cultures show significant increase in the percentage of active channels over time with no significant difference between the cultures (Figure 2c). However, using the microfluidic device, we found that both the tri- and co-cultures show significant increases in spike frequency from axons within the microchannels over time, and we observed significantly higher spike frequencies in the tri-culture at DIV 17 and 21 ( $p = 0.016$  and  $p = 0.0017$  respectively; Figure 2d). Additionally, we observed no differences among other electrophysiological features (percentage spikes in bursts, burst duration, and within burst ISI; Figure S2) and spike train synchrony (Figure 2e) between the tri- and co-cultures, once again suggesting minimal differences in culture maturation and stability between the tri- and co-cultures, with the exception of an increased spike frequency in the tri-culture.

### 3.3. Synaptic Density

As microglia are known to play a significant role in synapse formation and elimination during postnatal development [44–46], we compared synapse formation between the tri- and co-cultures over 21 DIV (Figure 3a). A two-way ANOVA revealed that there was no significant interaction between the culture type and the time in the culture on the density of post-synaptic marker PSD-95 (Figure 3b) and excitatory pre-synaptic marker VGlut1 (Figure 3c) puncta ( $p = 0.46$  and  $p = 0.36$  respectively). A simple main effects analysis revealed no significant difference between the density of PSD-95 and Vglut1 puncta based on the culture ( $p = 0.26$  and  $p = 0.15$  respectively), but it did reveal a significant difference based on the time in the culture ( $p = 0.0032$  and  $p = 0.0015$  respectively). We also compared the number of co-localized puncta as a measurement of mature excitatory synapses [47,48] (Figure 3d). Once again, a two-way ANOVA revealed no significant interactions between the culture type and the time in the culture on the number of mature excitatory synapses ( $p = 0.22$ ), and a simple main effects analysis revealed a significant difference increase in mature excitatory synapses based on the time in the culture ( $p = 0.0066$ ), but not based on culture type ( $p = 0.21$ ).

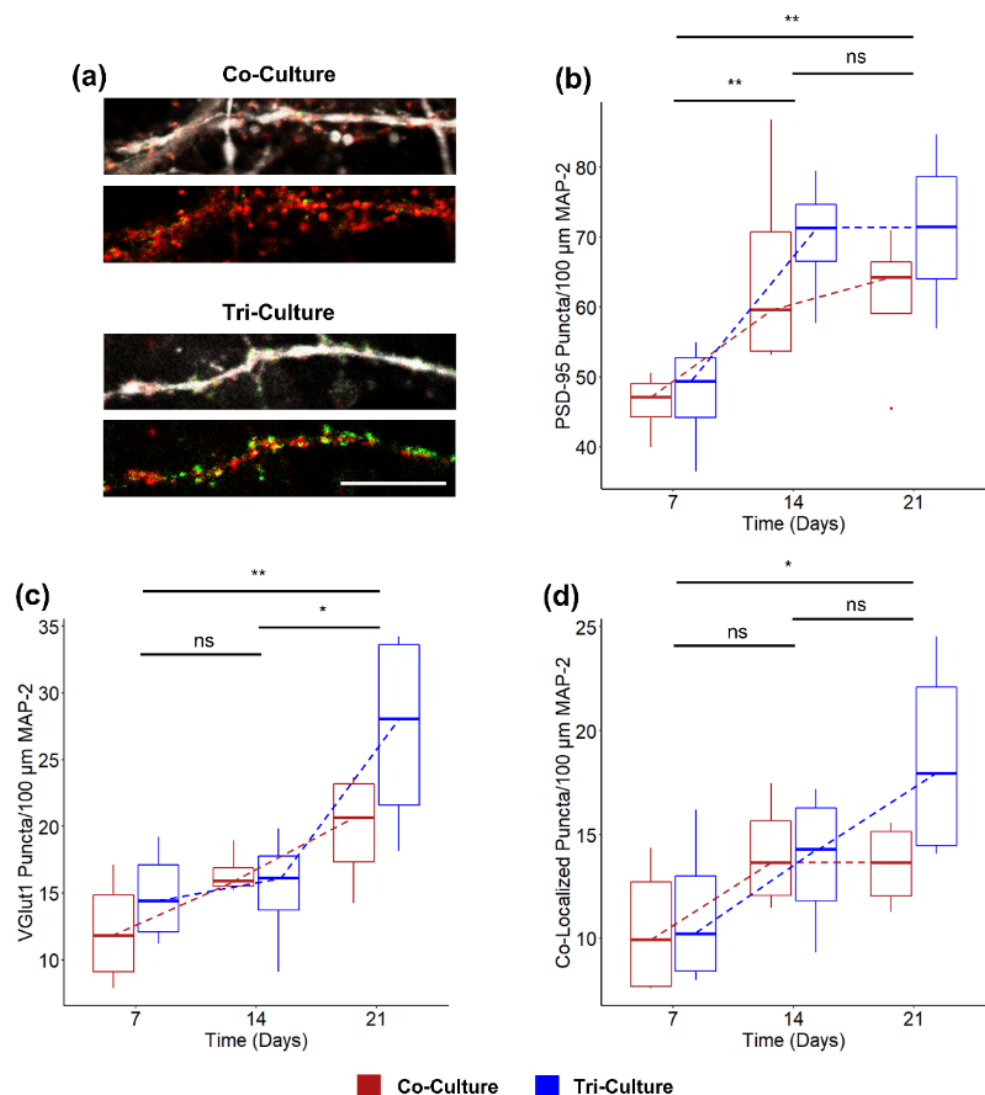


**Figure 3.** (a) Representative fluorescence images of co- and tri-cultures at DIV 21. The cultures are stained for the excitatory pre-synaptic marker VGluT1 (Green), post-synaptic marker PSD-95 (red). The above image also shows the co-localization with MAP-2 (white). (Scale bar = 10 μm). Comparison of the density of (b) PSD-95 puncta, (c) VGluT1 puncta, and (d) co-localized puncta. In all, three cases, a two-way ANOVA found no interaction between culture type and time in culture. Therefore, the asterisk indicates the significance of the main effect between timepoints ( $n = 4$ , from two independent dissections). \*  $p < 0.05$ , \*\*  $p < 0.01$ , ns indicates no significant difference. Trendlines are visual guides only.

### 3.4. Excitatory vs. Inhibitory Neurons

While we did not observe any statistically significant differences in synapse formation between the tri- and co-culture (Figure 3d), we saw trends of increased excitatory synapse formation at DIV 21 compared to DIV 7 in the tri-culture (Figure 3d) and a significant increase in spike frequency in the tri-culture (Figure 2d). As the cortex contains both excitatory and inhibitory neurons, we asked if the aforementioned differences could be attributed to changes in the ratio of excitatory to inhibitory neurons (E/I ratio). We found a bimodal distribution of the peak-trough duration of the averaged spike waveforms from 249 units recorded from both tri- and co-cultures (Figure S3). The first peak is centered at a peak-trough duration of ~220 μs, which correlates well with narrow-spiking inhibitory interneurons, while the second peak is centered at a peak-trough duration of ~380 μs, which correlated with broad-spiking excitatory neurons [49–51]. Additionally, the average



spike waveforms from these two groups correlated well with previously described narrow-spiking and broad-spiking waveforms (Figure 4a) [50,51]. Using the density histogram as a guide, we classified units as either inhibitory (peak-trough duration < 280  $\mu$ s) or excitatory (peak-trough duration > 280  $\mu$ s). We observed a significant increase in E/I ratio of recorded units in the tri-culture ( $86.91 \pm 3.27\%$  excitatory neurons) as compared to the co-culture ( $68.83 \pm 5.55\%$  excitatory neurons;  $p = 0.016$ ), as shown in Figure 4b. Interestingly, the E/I ratio of the tri-culture more closely resembles the E/I ratio of the cortex in vivo (~80% excitatory) [52].

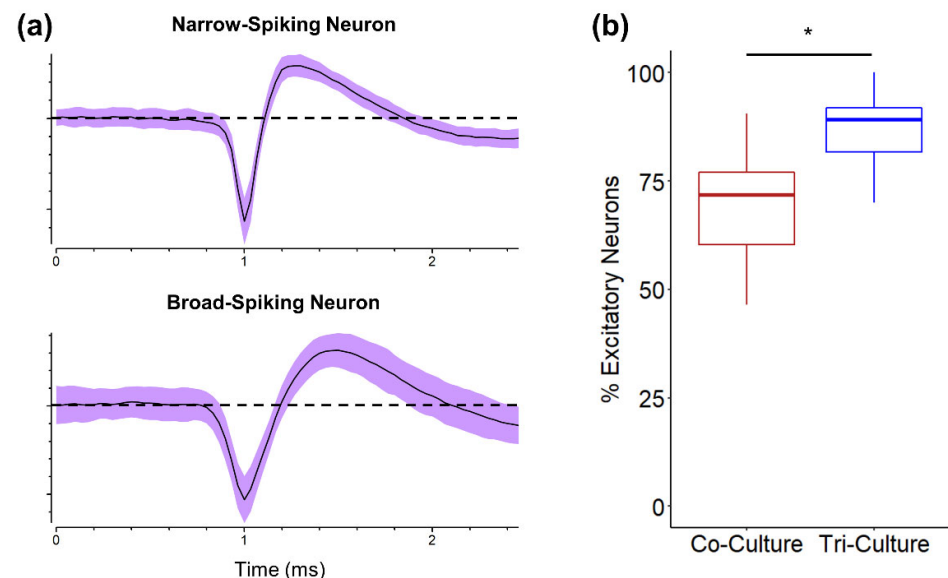


**Figure 4.** Comparison of the E/I ratio in tri- and co-cultures at DIV 21. (a) Representative waveforms of narrow-spiking and broad-spiking neurons recorded at DIV 21. The line represents the average spike waveform, while the shaded region is one standard deviation. (b) Percent excitatory neurons in the tri- and co-cultures at DIV 21 ( $n = 8$  MEAs (249 total units) from three independent dissections). \*  $p < 0.05$ .

### 3.5. Influence of LPS Exposure

In order to demonstrate the ability to detect changes in neural activity in response to neuroinflammatory stimuli, we challenged both co- and tri-cultures with 5  $\mu$ g/mL LPS at DIV 21. As expected, there was no change in the neural activity in the co-culture in response to LPS, as LPS acts through the toll-like Receptor 4 (TLR4), which is primarily expressed by microglia. Conversely, we observed a significant decrease in both active channels (Figure 5a) and spike frequency (Figure 5b) in the tri-culture following exposure to LPS. Additionally, we began to see a trend towards a reduction in spike frequency beginning at 3 h ( $p = 0.17$ ) before there was any change in the number of active channels ( $p = 0.71$ ). We were unable to compare other electrophysiological features (the percentage of spikes in bursts, burst duration, and within burst ISI) and spike train synchrony due to the dramatic reduction in active channels in the tri-culture following exposure to LPS limiting our ability to effectively characterize these features.

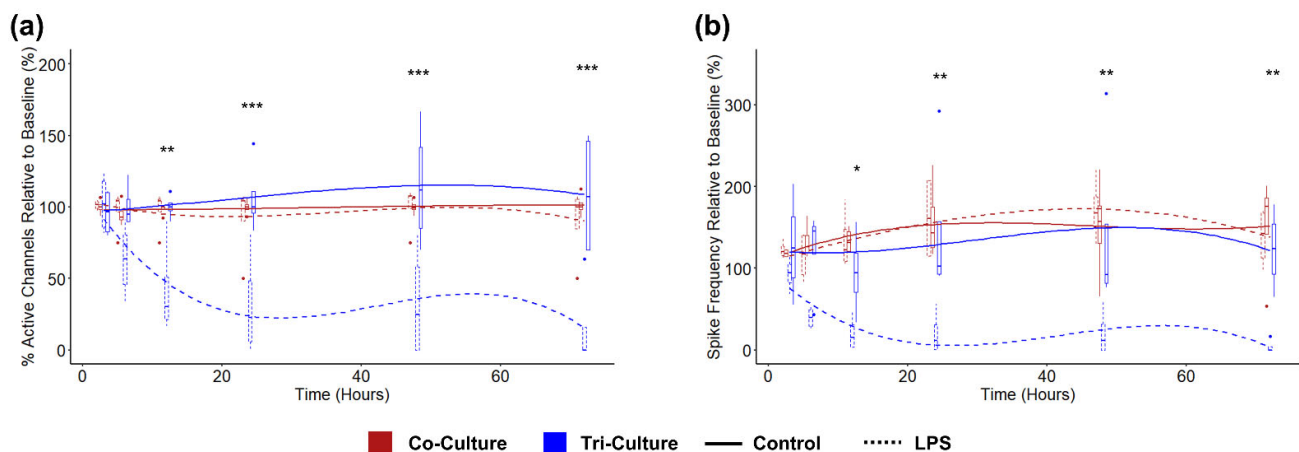


**Figure 5.** Comparing the change in (a) percent active channels and (b) spike frequency following exposure to 5  $\mu\text{g/mL}$  LPS between co-cultures (red) and tri-cultures (blue). The lines show the fitted liner mixed effects model (treating individual cultures as a random effect) with a b-spline basis. Asterisks indicate a significant difference in the estimated marginal means of the fitted curves between control and LPS treated tri-cultures at that timepoint ( $n = 4$ , from two independent dissections). \*  $p < 0.05$ , \*\*  $p < 0.01$ , \*\*\*  $p < 0.001$ .

#### 4. Discussion

Extracellular recording techniques using MEAs are a powerful tool to study *in vitro* neural cultures as they provide a non-invasive method to simultaneously record neural activity from multiple neurons within a culture. This makes them a popular method to study the changes in neural activity over time, as multiple recordings can be taken from the same culture to monitor changes during neural network formation [10,11] or in response to neurotoxic compounds [12–14]. In this study, we characterized the neural network maturation and electrophysiological response to neuroinflammatory stimuli of a recently described tri-culture that contains neurons, astrocytes, and microglia at physiologically relevant proportions [32] and has been shown to better mimic the *in vivo* neuroinflammatory response [32,33,53]. Additionally, we compared the neural activity of the tri-culture to a neuron-astrocyte co-culture model that is commonly used to study neurotoxic and neuroinflammatory challenges [23,54,55] to not only ensure that the presence of microglia in the tri-culture do not negatively impact the overall health of the neurons, but also to determine if it may influence neural activity or network formation, as microglia are known to play a significant role in synapse formation and plasticity [46,56,57]. As expected, we observed many of the common indicators of neural network formation and maturation, including an increase in the number of active channels, increased spike frequency, and increased synchrony in both the tri- and co-culture over time (Figure 1), indicating that the microglia within the tri-culture did not disrupt culture maturation or health. Similarly, we observed no significant differences between the tri- and co-cultures when comparing any of the aforementioned indicators of culture maturation (Figure 1) or other electrophysiological features (Figure S1) at any timepoint, which was somewhat surprising considering the significant role microglia is known to play in synaptic plasticity. One reason for this could be the relatively young microglia from perinatal pups used in this study. It has been shown that microglia function and transcriptome evolve significantly with age [58,59]; future studies can provide insight into electrophysiological manifestations of microglia age by systematically adding microglia from older animals to the baseline co-culture [60]. Nevertheless, we did see a trend towards increased neuronal network maturation in the tri-culture, as the synchrony of the tri-culture was increased at earlier timepoints (DIV 10,  $p = 0.11$ ), but this increase was not statistically significant (Figure 1g). Additionally, we saw some evidence that the tri-culture had an increase in spike frequency at DIV 21, as only the tri-culture showed a significant increase in spike frequency between DIV 7 and DIV 21

( $p = 0.0076$  vs.  $p = 0.51$  for the co-culture), but once again, there was no significant difference in spike frequency between the tri- and co-cultures at DIV 21 (Figure 1f). A recent study using a similar tri-culture showed a reversed trend, with microglia appearing to reduce spike frequency and other electrophysiological features [61]. However, in that paper, the amount of microglia was increased to 15–25% of the total cell population, which is more than double the number of microglia found in our tri-culture model (Figure S4) [32] and the proportions found in vivo [62]. Furthermore, the authors found that increased microglia reactivity corresponds with increasing microglia density, suggesting that the decrease in spike frequency may be a function of reactive microglia as opposed to more homeostatic microglia and would be in line with the results we obtained from our LPS-treated cultures.

In order to further investigate the potential difference in spike frequency, we cultured both the tri- and co-cultures in microfluidic devices, which have previously been shown to improve electrophysiological recording fidelity [31]. These devices consist of two cell culture chambers connected by a series of small microchannels with an integrated MEA. The small cross-sectional area of the microchannels prevents the cell bodies of neurons and glia from entering the microchannels but permits axons to pass through and synaptically connect the two neural cultures. Additionally, the spatial confinement forces axons in close approximation to electrodes placed underneath the microchannels, and the reduced volume within the microchannels reduces ionic dispersion, leading to an increase in spike amplitude [63], which leads to an overall improvement in recording fidelity. This enhancement in recording fidelity allowed us to not only observe the expected increase in spike frequency in both the tri- and co-cultures indicative of culture maturation [64,65], but also revealed a significant increase in the spike frequency of the tri-culture at later timepoints (Figure 2d), which is in line with the observations from the recordings taken from standard MEAs (Figure 1f). Furthermore, the incorporation of the tri-culture into the microfluidic device was straightforward, as it only required the use of a specialized culture medium, highlighting the tri-culture's amenability to complex culture setups such as microfluidic devices and organ-on-a-chip platforms.

In order to determine the cause of increased spike frequency in the tri-culture at later timepoints, we compared the number of pre-synaptic and excitatory post-synaptic puncta in the tri- and co-cultures, as microglia are known to play a significant role in synaptic formation and elimination during postnatal development [45,46]. Interestingly, a two-way ANOVA did not establish an interaction between time in culture and culture type (tri- vs. co-culture) when comparing the density of pre-synaptic, excitatory post-synaptic, or co-localized puncta (Figure 3b–d). Additionally, a main effects analysis did not reveal a significant difference between the tri- and co-cultures for any of the conditions. This was an unexpected finding as previous in vitro studies have shown that IL-10 secreted from microglia increase spine density and excitatory synapses [66]. However, in that study, the microglia and neurons were physically separated, with the microglia grown on a porous insert that was added to the isolated neuron culture at a later timepoint, preventing their physical contact. In addition, it has been shown that direct microglia contact with synapses can lead to synaptic elimination [67,68]. While we did not observe a significant difference between the tri- and co-culture, we noted a trend towards increased excitatory post-synaptic puncta at DIV 21 in the tri-culture (Figure 3c). Additionally, we observed that the tri-culture continues to show an increased co-localized puncta over the 21 DIV, while the number of co-localized puncta appears to plateau at DIV 14 (Figure 3d). The fact that we did not observe a significant difference in synaptic density and excitatory pre-synaptic puncta between the tri- and co-cultures may be due to the fact that the microglia and neurons are in close approximation in the tri-culture, leading to a balance of increased synaptogenesis due to IL-10 secretion by microglia and synaptic pruning due to the direct contact of microglia and synapses. Furthermore, astrocytes have also been shown to play a significant role in synaptic plasticity [69], and since both the tri- and co-cultures contain astrocytes, the influence of the microglia may be less apparent.

We also investigated the E/I ratio as a potential cause of the increased spike frequency and found that we recorded from a significantly higher percentage of broad-spiking excitatory neurons in the tri-culture (Figure 4b). Additionally, the E/I ratio of the tri-culture was much closer to the E/I ratio found in vivo [52]. However, we cannot be sure if this apparent increase in excitatory neurons in the tri-culture is due to an actual increase in the number of excitatory neurons in the tri-culture or due to a relative increase in the number of excitatory neurons incorporated into the neural network. It has been shown that GABAergic neurons may be less healthy than glutamatergic neurons in culture [70], and it may be possible that the microglia in the tri-culture are inducing apoptosis in the weakened GABAergic neurons. Alternatively, it has also been shown that glutamatergic neurons are much more dependent on glial support to establish functional glutamatergic synapses [70]. Therefore, the presence of microglia in the tri-culture may further enhance the incorporation of excitatory neurons into the neural network. Additionally, microglia are known to regulate perineuronal nets (PNNs), which stabilize synapses and have been shown to appear in cortical neuron cultures [71]. These PNNs primarily associate with narrow-spiking inhibitory neurons, leading to their over-incorporation into neural networks when microglia are not present [45]. Since microglia are present in the tri-culture, they may be able to regulate the PNNs, thereby allowing for an increased incorporation of excitatory neurons into the neural network and increasing the apparent E/I ratio to values closer to what is observed in vivo. Additionally, while the use of spike width is a classic characteristic used to classify excitatory versus inhibitory neurons [72] a few studies have also indicated that some pyramidal neurons can display a range of spike widths [73]. Additional studies comparing the proportion of VGlut1+ versus VGAT+ neurons would be beneficial to help verify the results from the extracellular recording characterizations.

Finally, we investigated the tri-culture's ability to detect changes in neural activity in response to neuroinflammatory stimuli. Therefore, we challenged the tri- and co-culture with 5 µg/mL of LPS and monitored the change in neural activity over 72 h. LPS is a well-characterized activator of neurotoxic neuroinflammation that acts through the TLR4, which is found on microglia but not neurons and astrocytes [74,75]. The activation of microglia by LPS leads to the secretion of proinflammatory cytokines [32,76], neuronal apoptosis [77,78], and the induction of a neurotoxic "A1" astrocyte phenotype [79]. Additionally, we have demonstrated a significant increase in apoptosis and cell death in tri-cultures treated with 5 µg/mL of LPS at 48 h [32,33]. Consequently, we observed a sharp decrease in both the number of active channels and spike frequency in the LPS-treated tri-cultures that became significant by 12 h post-exposure (Figure 5). Additionally, we observed that the spike frequency decreases at a more rapid rate than the number of active channels, suggesting that changes in neural activity can be detected prior to changes in cell viability. Furthermore, we only observe an ~10% increase in cytotoxicity (Figure S5) in the tri-culture following LPS exposure, which is significantly less than ~90% decrease in the active channels we observe in the same timeframe. This suggests that the extracellular recordings from the tri-culture are able to capture changes in neural activity in response to a neuroinflammatory stimuli, and the changes in activity cannot be attributed solely to neural death. This observation can be paralleled to the findings from the recent study that showed a decrease in electrophysiological activity with increasing microglia density in a dose-response manner [61], where higher microglia numbers in the culture lead to increased microglia reactivity, partially mimicking increased reactivity due to the LPS treatment here.

While we propose that this tri-culture is a powerful tool to study neuroinflammation, it is not without its limitations. Most notably is that microglia display significant heterogeneity both spatially and temporally within the CNS, which may not be fully captured within our model [80]. Additionally, the gene expression profile of cultured microglia has been shown to change over time [36], and, therefore, future work exploring changes in cellular heterogeneity over time would be beneficial to fully characterize the microglia population and the potential changes over time and help elucidate the true proportion of



inhibitory to excitatory neurons. Furthermore, while neurons, astrocytes, and microglia are the three CNS-specific cells most associated with neuroinflammation, other cells such as oligodendrocyte precursor cells (OPCs) and mature oligodendrocytes (OLs) are known to influence the neuroinflammatory response [81,82]. The tri-culture does contain a small number of both OPCs [32] and OLs (Figure S4). However, increasing their numbers to physiologically relevant densities would increase the physiological relevancy of the culture. It has also been shown that the additional factors added to the tri-culture medium can have direct effects on neurons and astrocytes in the culture [83–85], and it is possible that these effects could influence our reported results. However, we have previously demonstrated that cultures maintained using co-culture media with TGF- $\beta$  and cholesterol (but lacking IL-34 to ensure no microglia are present) show a nearly identical cell viability to native neuron-astrocyte co-cultures as compared to the significantly increased viability in the full tri-culture condition [33]. Similarly, we observed that cultures maintained with co-culture media with TGF- $\beta$  and cholesterol show a similar pattern of synaptic density as the native co-culture condition at DIV21 (Figure S6), which suggests that the presence of microglia within the tri-culture has a significantly larger effect on the observed outcomes than any direct effects on the neurons or astrocytes by the additional tri-culture factors. Finally, we cannot entirely rule out the impact of indirect effects, such as small changes in pH or the metabolic load, the presence of microglia may have had on the observed results. However, once again, we believe that these effects would be minor compared to the direct effects of the presence of microglia within the tri-culture. Ultimately, we believe that this study demonstrates that monitoring extracellular recordings from MEAs in combination with the described tri-culture of neurons, astrocytes, and microglia is a powerful method to non-invasively study the effect of neuroinflammation *in vitro*.

## 5. Conclusions

In this study, we characterized the neural activity and network maturation in a tri-culture of neurons, astrocytes, and microglia. We showed that the presence of microglia in the tri-culture had minimal impact on the formation and stability of neural networks, with the exception of an increase in spike frequency in the tri-culture. Additionally, the characterization of the average spike waveforms revealed that the tri-culture had an E/I ratio much closer to that found in the rat cortex. Finally, we demonstrated that the more biologically relevant neuroinflammatory response of the tri-culture can be captured via extracellular recordings as indicated by a significant decrease in both active channels and spike frequency following exposure to LPS. We expect that the electrophysiological read-out from the tri-culture will be useful for continuous and non-invasive studies in the context of neuroinflammation, neurodevelopment, and neurodegeneration, where the presence of microglia imparts the ability to capture both neurotoxic and neuroprotective phenomena observed *in vivo*.

**Supplementary Materials:** The following supporting information can be downloaded at: <https://www.mdpi.com/article/10.3390/cells12050821/s1>, Supplementary materials document includes data on additional electrophysiological, synaptic density, and cell viability analyses contrasting the co-culture and tri-culture configurations, as well as micrographs and analysis of microglia and oligodendrocytes in the tri-culture.

**Author Contributions:** N.G. and E.S.; designed the experiments. N.G.; performed device fabrication, cell culture, electrophysiological recordings, imaging, and data analysis and wrote the main manuscript text. G.G.; contributed to the development and fabrication of microfluidic devices and microelectrode arrays, and data analysis. H.K.; conducted confocal microscopy. A.G.; contributed to electrophysiological data analysis. E.S.; contributed to the interpretation of experimental results and edited the manuscript. All authors have read and agreed to the published version of the manuscript.

**Funding:** We gratefully acknowledge the support from the National Institutes of Health via NINDS/NIA R03-NS118156, NIBIB R21-EB024635, and NCCIH R21-AT010933, and from the National Science Foundation via CBET-1454426 and DMR-2003849. NG was partially supported by the UC Davis Biotechnology Training Program award.

**Institutional Review Board Statement:** All procedures involving animals were conducted in accordance with the National Institutes of Health Guide for the Care and Use of Laboratory Animals following the protocol #22421 approved on 4 August 2022 by the University of California, Davis Institutional Animal Care and Use Committee.

**Informed Consent Statement:** Not applicable.

**Data Availability Statement:** The datasets generated during and/or analyzed during the current study are available from the corresponding author on reasonable request.

**Acknowledgments:** This project benefited from the resources of the MIND Institute IDDRC Core services (NICHD P50-HD103526) and University of California, Davis-Center for Nano/Micro-Manufacturing facility.

**Conflicts of Interest:** The authors declare that they have no competing interests.

## Abbreviations

MEA	Microelectrode array
E/I ratio	Excitatory-to-inhibitory-neuron ratio
LPS	Lipopolysaccharide
CNS	Central nervous system
TLR	Toll-like receptor
DIV	Days in vitro
PDMS	Polydimethylsiloxane
PECVD	Plasma enhanced chemical vapor deposition
IL	Interleukin
TGF- $\beta$	Transforming growth factor beta
DPBS+	Dulbecco's phosphate buffered saline solution with calcium and magnesium
PFA	Paraformaldehyde
PSD-95	Postsynaptic Density Protein 95
VGlut1	Vesicular Glutamate Transporter 1
MAP2	Microtubule-associated Protein 2
GFAP	Glial fibrillary acidic protein
Iba-1	Ionized Calcium-binding Adaptor Molecule 1
DAPI	4',6-diamidino-2-phenylindole
SEM	Standard error of the mean
ANOVA	Analysis of variance
TLR4	Toll-like Receptor 4
PNN	Perineuronal nets

## References

1. Naegel, M.; Martin, R. *The Good and the Bad of Neuroinflammation in Multiple Sclerosis*, 1st ed.; Handbook of Clinical Neurology; Elsevier B.V.: Amsterdam, The Netherlands, 2014. [\[CrossRef\]](#)
2. Calsolaro, V.; Edison, P. Neuroinflammation in Alzheimer's disease: Current evidence and future directions. *Alzheimer's Dement.* **2016**, *12*, 719–732. [\[CrossRef\]](#) [\[PubMed\]](#)
3. Hirsch, E.C.; Vyas, S.; Hunot, S. Neuroinflammation in Parkinson's disease. *Park. Relat. Disord.* **2012**, *18*, 210–212. [\[CrossRef\]](#) [\[PubMed\]](#)
4. Jayaraj, R.L.; Azimullah, S.; Beiram, R.; Jalal, F.Y.; Rosenberg, G.A. Neuroinflammation: Friend and foe for ischemic stroke. *J. Neuroinflamm.* **2019**, *16*, 142. [\[CrossRef\]](#) [\[PubMed\]](#)
5. Polikov, V.S.; Tresco, P.A.; Reichert, W.M. Response of brain tissue to chronically implanted neural electrodes. *J. Neurosci. Methods* **2005**, *148*, 1–18. [\[CrossRef\]](#)
6. Li, Q.; Barres, B.A. Microglia and macrophages in brain homeostasis and disease. *Nat. Rev. Immunol.* **2017**, *18*, 225–242. [\[CrossRef\]](#)
7. Simard, M.; Nedergaard, M. The neurobiology of glia in the context of water and ion homeostasis. *Neuroscience* **2004**, *129*, 877–896. [\[CrossRef\]](#)

8. Potter, S.M.; DeMarse, T.B. A New Approach to Neural Cell Culture for Long-Term Studies. *J. Neurosci. Methods* **2001**, *110*, 17–24. Available online: <https://linkinghub.elsevier.com/retrieve/pii/S0165027001004125> (accessed on 26 September 2022). [\[CrossRef\]](#)
9. Kim, R.; Joo, S.; Jung, H.; Hong, N.; Nam, Y. Recent trends in microelectrode array technology for in vitro neural interface platform. *Biomed. Eng. Lett.* **2014**, *4*, 129–141. [\[CrossRef\]](#)
10. Frank, C.L.; Brown, J.P.; Wallace, K.; Mundy, W.R.; Shafer, T.J. Developmental neurotoxicants disrupt activity in cortical networks on microelectrode arrays: Results of screening 86 compounds during neural network formation. *Toxicol. Sci.* **2017**, *160*, 121–135. [\[CrossRef\]](#)
11. Shafer, T.J.; Brown, J.P.; Lynch, B.; Davila-Montero, S.; Wallace, K.; Friedman, K.P. Evaluation of chemical effects on network formation in cortical neurons grown on microelectrode arrays. *Toxicol. Sci.* **2019**, *169*, 436–455. [\[CrossRef\]](#)
12. Johnstone, A.F.M.; Gross, G.W.; Weiss, D.G.; Schroeder, O.H.U.; Gramowski, A.; Shafer, T.J. Microelectrode arrays: A physiologically based neurotoxicity testing platform for the 21st century. *Neurotoxicology* **2010**, *31*, 331–350. [\[CrossRef\]](#)
13. Gopal, K.V. Neurotoxic effects of mercury on auditory cortex networks growing on microelectrode arrays: A preliminary analysis. *Neurotoxicol. Teratol.* **2003**, *25*, 69–76. [\[CrossRef\]](#)
14. Novellino, A.; Scelfo, B.; Palosaari, T.; Price, A.; Sobanski, T.; Shafer, T.J.; Johnstone, A.F.; Gross, G.W.; Gramowski, A.; Schroeder, O.; et al. Development of micro-electrode array based tests for neurotoxicity: Assessment of interlaboratory reproducibility with neuroactive chemicals. *Front. Neuroeng.* **2011**, *4*, 1–14. [\[CrossRef\]](#)
15. Charkhkar, H.; Meyyappan, S.; Matveeva, E.; Moll, J.R.; McHail, D.G.; Peixoto, N.; Cliff, R.O.; Pancrazio, J.J. Amyloid beta modulation of neuronal network activity in vitro. *Brain Res.* **2015**, *1629*, 1–9. [\[CrossRef\]](#)
16. Gao, F.; Gao, K.; He, C.; Liu, M.; Wan, H.; Wang, P. Multi-site dynamic recording for A $\beta$  oligomers-induced Alzheimer's disease in vitro based on neuronal network chip. *Biosens. Bioelectron.* **2019**, *133*, 183–191. [\[CrossRef\]](#)
17. Amin, H.; Nieus, T.; Lonardoni, D.; Maccione, A.; Berdondini, L. High-resolution bioelectrical imaging of A $\beta$ -induced network dysfunction on CMOS-MEAs for neurotoxicity and rescue studies. *Sci. Rep.* **2017**, *7*, 1–13. [\[CrossRef\]](#)
18. Belle, A.M.; Enright, H.A.; Sales, A.P.; Kulp, K.; Osburn, J.; Kuhn, E.A.; Fischer, N.O.; Wheeler, E.K. Evaluation of in vitro neuronal platforms as surrogates for in vivo whole brain systems. *Sci. Rep.* **2018**, *8*, 1–9. [\[CrossRef\]](#)
19. Chapman, C.A.R.; Chen, H.; Stamou, M.; Biener, J.; Biener, M.M.; Lein, P.J.; Seker, E. Nanoporous gold as a neural interface coating: Effects of topography, surface chemistry, and feature size. *ACS Appl. Mater. Interfaces* **2015**, *7*, 7093–7100. [\[CrossRef\]](#)
20. Xiang, G.; Pan, L.; Huang, L.; Yu, Z.; Song, X.; Cheng, J.; Xing, W.; Zhou, Y. Microelectrode array-based system for neuropharmacological applications with cortical neurons cultured in vitro. *Biosens. Bioelectron.* **2007**, *22*, 2478–2484. [\[CrossRef\]](#)
21. James, C.; Spence, A.; Dowell-Mesfin, N.; Hussain, R.; Smith, K.; Craighead, H.; Isaacson, M.; Shain, W.; Turner, J. Extracellular recordings from patterned neuronal networks using planar microelectrode arrays. *IEEE Trans. Biomed. Eng.* **2004**, *51*, 1640–1648. [\[CrossRef\]](#)
22. Nam, Y.; Wheeler, B.C.; Heuschkel, M.O. Neural recording and stimulation of dissociated hippocampal cultures using microfabricated three-dimensional tip electrode array. *J. Neurosci. Methods* **2006**, *155*, 296–299. [\[CrossRef\]](#) [\[PubMed\]](#)
23. Chapman, C.A.R.; Wang, L.; Chen, H.; Garrison, J.; Lein, P.J.; Seker, E. Nanoporous Gold Biointerfaces: Modifying Nanostructure to Control Neural Cell Coverage and Enhance Electrophysiological Recording Performance. *Adv. Funct. Mater.* **2016**, *27*, 1604631. [\[CrossRef\]](#) [\[PubMed\]](#)
24. Enright, H.A.; Lam, D.; Sebastian, A.; Sales, A.P.; Cadena, J.; Hum, N.R.; Osburn, J.J.; Peters, S.K.G.; Petkus, B.; Soscia, D.A.; et al. Functional and transcriptional characterization of complex neuronal co-cultures. *Sci. Rep.* **2020**, *10*, 1–14. [\[CrossRef\]](#) [\[PubMed\]](#)
25. Napoli, A.; Obeid, I. Comparative Analysis of Human and Rodent Brain Primary Neuronal Culture Spontaneous Activity Using Micro-Electrode Array Technology. *J. Cell Biochem.* **2016**, *117*, 559–565. [\[CrossRef\]](#) [\[PubMed\]](#)
26. Odawara, A.; Saitoh, Y.; Alhebshi, A.; Gotoh, M.; Suzuki, I. Long-term electrophysiological activity and pharmacological response of a human induced pluripotent stem cell-derived neuron and astrocyte co-culture. *Biochem. Biophys. Res. Commun.* **2014**, *443*, 1176–1181. [\[CrossRef\]](#)
27. Heikkilä, T.J.; Ylä-Outinen, L.; Tanskanen, J.M.; Lappalainen, R.S.; Skottman, H.; Suuronen, R.; Mikkonen, J.E.; Hyttinen, J.A.; Narkilahti, S. Human embryonic stem cell-derived neuronal cells form spontaneously active neuronal networks in vitro. *Exp. Neurol.* **2009**, *218*, 109–116. [\[CrossRef\]](#)
28. Soscia, D.A.; Lam, D.; Tooker, A.C.; Enright, H.A.; Triplett, M.; Karande, P.; Peters, S.K.G.; Sales, A.P.; Wheeler, E.K.; Fischer, N.O. A flexible 3-dimensional microelectrode array for: In vitro brain models. *Lab. Chip. R. Soc. Chem.* **2020**, *20*, 901–911. [\[CrossRef\]](#)
29. Shin, H.; Jeong, S.; Lee, J.-H.; Sun, W.; Choi, N.; Cho, I.-J. 3D high-density microelectrode array with optical stimulation and drug delivery for investigating neural circuit dynamics. *Nat. Commun.* **2021**, *12*, 1–18. [\[CrossRef\]](#)
30. Dauth, S.; Maoz, B.M.; Sheehy, S.P.; Hemphill, M.A.; Murty, T.; Macedonia, M.K.; Greer, A.M.; Budnik, B.; Parker, K.K. Neurons derived from different brain regions are inherently different in vitro: A novel multiregional brain-on-a-chip. *J. Neurophysiol.* **2017**, *117*, 1320–1341. [\[CrossRef\]](#)
31. Goshi, N.; Girardi, G.; Souza, F.D.C.; Gardner, A.; Lein, P.J.; Seker, E. Influence of microchannel geometry on device performance and electrophysiological recording fidelity during long-term studies of connected neural populations. *Lab. Chip* **2022**, *22*, 3961–3975. [\[CrossRef\]](#)
32. Goshi, N.; Morgan, R.K.; Lein, P.J.; Seker, E. A primary neural cell culture model to study neuron, astrocyte, and microglia interactions in neuroinflammation. *J. Neuroinflamm.* **2020**, *17*, 1–16. [\[CrossRef\]](#)

33. Goshi, N.; Kim, H.; Seker, E. Primary Cortical Cell Tri-Culture-Based Screening of Neuroinflammatory Response in Toll-like Receptor Activation. *Biomedicines* **2022**, *10*, 2122. [\[CrossRef\]](#)
34. Gattenplan, K.A.; Liddelow, S.A. Astrocytes and Microglia: Models and Tools. *J. Exp. Med.* **2018**, *216*, 71–83. [\[CrossRef\]](#)
35. Taylor, A.M.; Rhee, S.W.; Tu, C.H.; Cribbs, D.H.; Cotman, C.W.; Jeon, N.L. Microfluidic multicompartiment device for neuroscience research. *Langmuir* **2003**, *19*, 1551–1556. [\[CrossRef\]](#)
36. Bohlen, C.J.; Bennett, F.C.; Tucker, A.F.; Collins, H.Y.; Mulinyawe, S.B.; Barres, B.A. Diverse Requirements for Microglial Survival, Specification, and Function Revealed by Defined-Medium Cultures. *Neuron* **2017**, *94*, 759–773.e8. [\[CrossRef\]](#)
37. Wayman, G.A.; Bose, D.D.; Yang, D.; Lesiak, A.; Bruun, D.; Impey, S.; Ledoux, V.; Pessah, I.N.; Lein, P.J. PCB-95 modulates the calcium-dependent signaling pathway responsible for activity-dependent dendritic growth. *Environ. Health Perspect.* **2012**, *120*, 1003–1009. [\[CrossRef\]](#)
38. Kreuz, T.; Chicharro, D.; Houghton, C.; Andrzejak, R.G.; Mormann, F. Monitoring spike train synchrony. *J. Neurophysiol.* **2013**, *109*, 1457–1472. [\[CrossRef\]](#)
39. Mulansky, M.; Kreuz, T. PySpike—A Python library for analyzing spike train synchrony. *Software* **2016**, *5*, 183–189. [\[CrossRef\]](#)
40. Charlesworth, P.; Cotterill, E.; Morton, A.; Grant, S.G.; Eglen, S.J. Quantitative differences in developmental profiles of spontaneous activity in cortical and hippocampal cultures. *Neural Dev.* **2015**, *10*, 1–10. [\[CrossRef\]](#)
41. Sethi, S.; Keil, K.P.; Lein, P.J. 3,3'-Dichlorobiphenyl (PCB 11) Promotes Dendritic Arborization in Primary Rat Cortical Neurons via a CREB-Dependent Mechanism. *Arch. Toxicol.* **2018**, *92*, 3337–3345. [\[CrossRef\]](#)
42. Toivanen, M.; Pelkonen, A.; Mäkinen, M.; Ylä-Outinen, L.; Sukki, L.; Kallio, P.; Ristola, M.; Narkilahti, S. Optimised PDMS tunnel devices on MEAs increase the probability of detecting electrical activity from human stem cell-derived neuronal networks. *Front. Neurosci.* **2017**, *11*, 606. [\[CrossRef\]](#) [\[PubMed\]](#)
43. Wang, L.; Riss, M.; Buitrago, J.O.; Claverol-tintur, E. Biophysics of microchannel-enabled neuron-electrode interfaces. *Neural Eng.* **2012**, *9*, 26010. [\[CrossRef\]](#) [\[PubMed\]](#)
44. Hong, S.; Dissing-Olesen, L.; Stevens, B. New insights on the role of microglia in synaptic pruning in health and disease. *Curr. Opin. Neurobiol.* **2016**, *36*, 128–134. [\[CrossRef\]](#) [\[PubMed\]](#)
45. Crapser, J.D.; Arreola, M.A.; Tsourmas, K.I.; Green, K.N. Microglia as hackers of the matrix: Sculpting synapses and the extracellular space. *Cell Mol. Immunol.* **2021**, *18*, 2472–2488. [\[CrossRef\]](#)
46. Andoh, M.; Koyama, R. Microglia regulate synaptic development and plasticity. *Dev. Neurobiol.* **2021**, *81*, 568–590. [\[CrossRef\]](#)
47. Flavell, S.W.; Cowan, C.W.; Kim, T.-K.; Greer, P.L.; Lin, Y.; Paradis, S.; Griffith, E.C.; Hu, L.S.; Chen, C.; Greenberg, M.E. Activity-dependent regulation of MEF2 transcription factors suppresses excitatory synapse number. *Science* **2006**, *311*, 1008–1012. [\[CrossRef\]](#)
48. Verstraelen, P.; Barriga, G.G.-D.; Verschuuren, M.; Asselbergh, B.; Nuydens, R.; Larsen, P.H.; Timmermans, J.-P.; De Vos, W.H. Systematic Quantification of Synapses in Primary Neuronal Culture. *iScience* **2020**, *23*, 101542. [\[CrossRef\]](#)
49. Mitchell, J.F.; Sundberg, K.A.; Reynolds, J.H. Differential Attention-Dependent Response Modulation across Cell Classes in Macaque Visual Area V4. *Neuron* **2007**, *55*, 131–141. [\[CrossRef\]](#)
50. Wang, B.; Ke, W.; Guang, J.; Chen, G.; Yin, L.; Deng, S.; He, Q.; Liu, Y.; He, T.; Zheng, R.; et al. Firing frequency maxima of fast-spiking neurons in human, monkey, and mouse neocortex. *Front. Cell Neurosci.* **2016**, *10*, 239. [\[CrossRef\]](#)
51. Robbins, A.A.; Fox, S.E.; Holmes, G.L.; Scott, R.C.; Barry, J.M. Short duration waveforms recorded extracellularly from freely moving rats are representative of axonal activity. *Front. Neural Circuits* **2013**, *7*, 181. [\[CrossRef\]](#)
52. Sahara, S.; Yanagawa, Y.; O'Leary, D.D.M.; Stevens, C.F. The fraction of cortical GABAergic neurons is constant from near the start of cortical neurogenesis to adulthood. *J. Neurosci.* **2012**, *32*, 4755–4761. [\[CrossRef\]](#)
53. Jung, H.; Lee, S.Y.; Lim, S.; Choi, H.R.; Choi, Y.; Kim, M.; Kim, S.; Lee, Y.; Han, K.H.; Chung, W.-S.; et al. Anti-inflammatory clearance of amyloid- $\beta$  by a chimeric Gas6 fusion protein. *Nat. Med.* **2022**, *28*, 1802–1812. [\[CrossRef\]](#)
54. Jones, E.V.; Cook, D.; Murai, K.K. A Neuron-Astrocyte Co-Culture System to Investigate Astrocyte-Secreted Factors in Mouse Neuronal Development. In *Astrocytes*; Humana Press: Totoma, NJ, USA, 2012; pp. 341–352. ISBN 9781617794520.
55. Ozog, M.A.; Siushansian, R.; Naus, C.C.G. Blocked Gap Junctional Coupling Increases Glutamate-Induced Neurotoxicity in Neuron-Astrocyte Co-Cultures. *J. Neuropathol. Exp. Neurol.* **2002**, *61*, 132–141. [\[CrossRef\]](#)
56. Miyamoto, A.; Wake, H.; Ishikawa, A.W.; Eto, K.; Shibata, K.; Murakoshi, H.; Koizumi, S.; Moorhouse, A.J.; Yoshimura, Y.; Nabekura, J. Microglia contact induces synapse formation in developing somatosensory cortex. *Nat. Commun.* **2016**, *7*, 12540. [\[CrossRef\]](#)
57. Wu, Y.; Dissing-Olesen, L.; MacVicar, B.A.; Stevens, B. Microglia: Dynamic Mediators of Synapse Development and Plasticity. *Trends Immunol.* **2015**, *36*, 605–613. [\[CrossRef\]](#)
58. Spittau, B. Aging microglia-phenotypes, functions and implications for age-related neurodegenerative diseases. *Front. Aging Neurosci.* **2017**, *9*, 194. [\[CrossRef\]](#)
59. Pan, J.; Ma, N.; Yu, B.; Zhang, W.; Wan, J. Transcriptomic profiling of microglia and astrocytes throughout aging. *J. Neuroinflamm.* **2020**, *17*, 97. [\[CrossRef\]](#)
60. Luchena, C.; Zuazo-Ibarra, J.; Valero, J.; Matute, C.; Alberdi, E.; Capetillo-Zarate, E. A Neuron, Microglia, and Astrocyte Triple Co-culture Model to Study Alzheimer's Disease. *Front. Aging Neurosci.* **2022**, *14*, 271. [\[CrossRef\]](#)



61. Phadke, L.; Lau, D.H.W.; Aghaizu, N.D.; Ibarra, S.; Navarron, C.M.; Granat, L.; Magno, L.; Whiting, P.; Jolly, S. A primary rodent triculture model to investigate the role of glia-neuron crosstalk in regulation of neuronal activity. *Front. Aging Neurosci.* **2022**, *14*, 1–16. [\[CrossRef\]](#)
62. Von Bartheld, C.S.; Bahney, J.; Herculano-houzel, S. The Search for True Numbers of Neurons and Glial Cells in the Human Brain: A Review of 150 Years of Cell Counting. *J. Comp. Neurol.* **2016**, *524*, 3865–3895. [\[CrossRef\]](#)
63. Pan, L.; Alagapan, S.; Franca, E.; Demarse, T.; Brewer, G.J.; Wheeler, B.C. Large extracellular spikes recordable from axons in microtunnels. *IEEE Trans. Neural Syst. Rehabil. Eng.* **2014**, *22*, 453–459. [\[CrossRef\]](#) [\[PubMed\]](#)
64. Biffi, E.; Regalia, G.; Menegon, A.; Ferrigno, G.; Pedrocchi, A. The influence of neuronal density and maturation on network activity of hippocampal cell cultures: A methodological study. *PLoS ONE* **2013**, *8*, e83899. [\[CrossRef\]](#) [\[PubMed\]](#)
65. Wagenaar, D.A.; Pine, J.; Potter, S.M. An extremely rich repertoire of bursting patterns during the development of cortical cultures. *BMC Neurosci.* **2006**, *7*, 11. [\[CrossRef\]](#) [\[PubMed\]](#)
66. Lim, S.H.; Park, E.; You, B.; Jung, Y.; Park, A.R.; Park, S.G.; Lee, J.R. Neuronal synapse formation induced by microglia and interleukin 10. *PLoS ONE* **2013**, *8*, e81218. [\[CrossRef\]](#) [\[PubMed\]](#)
67. Wake, H.; Moorhouse, A.J.; Jinno, S.; Kohsaka, S.; Nabekura, J. Resting microglia directly monitor the functional state of synapses in vivo and determine the fate of ischemic terminals. *J. Neurosci.* **2009**, *29*, 3974–3980. [\[CrossRef\]](#)
68. Tremblay, M.É.; Lowery, R.L.; Majewska, A.K. Microglial interactions with synapses are modulated by visual experience. *PLoS Biol.* **2010**, *8*, e1000527. [\[CrossRef\]](#)
69. Perez-Catalan, N.A.; Doe, C.Q.; Ackerman, S.D. The role of astrocyte-mediated plasticity in neural circuit development and function. *Neural Dev.* **2021**, *16*, 1. [\[CrossRef\]](#)
70. Turko, P.; Groberman, K.; Browa, F.; Cobb, S.; Vida, I. Differential dependence of GABAergic and glutamatergic neurons on glia for the establishment of synaptic transmission. *Cereb. Cortex* **2019**, *29*, 1230–1243. [\[CrossRef\]](#)
71. Miyata, S.; Nishimura, Y.; Hayashi, N.; Oohira, A. Construction of perineuronal net-like structure by cortical neurons in culture. *Neuroscience* **2005**, *136*, 95–104. [\[CrossRef\]](#)
72. Paulk, A.C.; Kfir, Y.; Khanna, A.R.; Mustroph, M.L.; Trautmann, E.M.; Soper, D.J.; Stavisky, S.D.; Welkenhuysen, M.; Dutta, B.; Shenoy, K.V.; et al. Large-Scale Neural Recordings with Single Neuron Resolution Using Neuropixels Probes in Human Cortex. *Nat. Neurosci.* **2022**, *25*, 252–263. [\[CrossRef\]](#)
73. Vigneswaran, G.; Kraskov, A.; Lemon, R.N. Large Identified Pyramidal Cells in Macaque Motor and Premotor Cortex Exhibit “Thin Spikes”: Implications for Cell Type Classification. *J. Neurosci.* **2011**, *31*, 14235–14242. [\[CrossRef\]](#)
74. Nakamura, Y.; Si, Q.; Kataoka, K. Lipopolysaccharide-induced microglial activation in culture: Temporal profiles of morphological change and release of cytokines and nitric oxide. *Neurosci. Res.* **1999**, *35*, 95–100. [\[CrossRef\]](#)
75. Lehnardt, S.; Lachance, C.; Patrizi, S.; Lefebvre, S.; Follett, P.L.; Jensen, F.E.; Rosenberg, P.A.; Volpe, J.J.; Vartanian, T. The Toll-Like Receptor TLR4 Is Necessary for Lipopolysaccharide- Induced Oligodendrocyte Injury in the CNS. *J. Neurosci.* **2002**, *22*, 2478–2486. [\[CrossRef\]](#)
76. Kothur, K.; Wienholt, L.; Brilot, F.; Dale, R.C. CSF cytokines/chemokines as biomarkers in neuroinflammatory CNS disorders: A systematic review. *Cytokine* **2016**, *77*, 227–237. [\[CrossRef\]](#)
77. Nimmervoll, B.; White, R.; Yang, J.W.; An, S.; Henn, C.; Sun, J.J.; Luhmann, H.J. LPS-induced microglial secretion of TNF $\alpha$  increases activity-dependent neuronal apoptosis in the neonatal cerebral cortex. *Cereb. Cortex* **2013**, *23*, 1742–1755. [\[CrossRef\]](#)
78. Wang, X.; Chen, S.; Ma, G.; Ye, M.; Lu, G. Involvement of proinflammatory factors, apoptosis, caspase-3 activation and Ca<sup>2+</sup> disturbance in microglia activation-mediated dopaminergic cell degeneration. *Mech. Ageing Dev.* **2005**, *126*, 1241–1254. [\[CrossRef\]](#)
79. Liddelow, S.A.; Guttenplan, K.A.; Clarke, L.E.; Bennett, F.C.; Bohlen, C.J.; Schirmer, L.; Bennett, M.L.; Münch, A.E.; Chung, W.-S.; Peterson, T.C.; et al. Neurotoxic Reactive Astrocytes are Induced by Activated Microglia. *Nature* **2017**, *541*, 481–487. Available online: <http://www.nature.com/doi/10.1038/nature21029> (accessed on 3 March 2020). [\[CrossRef\]](#)
80. Masuda, T.; Sankowski, R.; Staszewski, O.; Prinz, M. Microglia Heterogeneity in the Single-Cell Era. *Cell Rep.* **2020**, *30*, 1271–1281. [\[CrossRef\]](#)
81. Dimou, L.; Gallo, V. NG2-Glia and Their Functions in the Central Nervous System. *Glia* **2015**, *63*, 1429–1451. [\[CrossRef\]](#)
82. Kassmann, C.M.; Lappe-Siefke, C.; Baes, M.; Brügger, B.; Mildner, A.; Werner, H.B.; Natt, O.; Michaelis, T.; Prinz, M.; Frahm, J.; et al. Axonal Loss and Neuroinflammation Caused by Peroxisome-Deficient Oligodendrocytes. *Nat. Genet.* **2007**, *39*, 969–976. [\[CrossRef\]](#)
83. Diniz, L.P.; Matias, I.C.P.; Garcia, M.N.; Gomes, F.C.A. Astrocytic Control of Neural Circuit Formation: Highlights on TGF- $\beta$  Signaling. *Neurochem. Int.* **2014**, *78*, 18–27. [\[CrossRef\]](#) [\[PubMed\]](#)
84. Pfrieger, F.W. Cholesterol Homeostasis and Function in Neurons of the Central Nervous System. *Cell. Mol. Life Sci.* **2003**, *60*, 1158–1171. [\[CrossRef\]](#) [\[PubMed\]](#)
85. Henrich-Noack, P.; Prehn, J.H.; Kriegstein, J. Neuroprotective Effects of TGF- $\beta$  1. *J. Neural Transm. Suppl.* **1994**, *43*, 33–45. [\[PubMed\]](#)

**Disclaimer/Publisher’s Note:** The statements, opinions and data contained in all publications are solely those of the individual author(s) and contributor(s) and not of MDPI and/or the editor(s). MDPI and/or the editor(s) disclaim responsibility for any injury to people or property resulting from any ideas, methods, instructions or products referred to in the content.